

A Dynamical Systems Approach to Damage Evolution Tracking, Part 1: Description and Experimental Application

David Chelidze

Department of Mechanical Engineering & Applied Mechanics,
University of Rhode Island,
Kingston, RI 02881
e-mail: chelidze@egr.uri.edu

Joseph P. Cusumano

Department of Engineering,
Science & Mechanics,
Pennsylvania State University,
University Park, PA 16802
e-mail: jpc@crash.esm.psu.edu

Anindya Chatterjee

Department of Mechanical Engineering,
Indian Institute of Science,
Bangalore, 560012, India
e-mail: anindya@mecheng.iisc.ernet.in

In this two-part paper we present a novel method for tracking a slowly evolving hidden damage process responsible for nonstationarity in a fast dynamical system. The development of the method and its application to an electromechanical experiment is the core of Part 1. In Part 2, a mathematical model of the experimental system is developed and used to validate the experimental results. In addition, an analytical connection is established between the tracking method and the physics of the system based on the idea of averaging and the slow flow equations for the hidden process. The tracking method developed in this study uses a nonlinear, two-time-scale modeling strategy based on the delay reconstruction of a system's phase space. The method treats damage-induced nonstationarity as evolving in a hierarchical dynamical system containing a fast, directly observable subsystem coupled to a slow, hidden subsystem. The utility of the method is demonstrated by tracking battery discharge in a vibrating beam system with a battery-powered electromagnetic restoring force. Applications to systems with evolving material damage are also discussed. [DOI: 10.1115/1.1456908]

1 Introduction

In this first part of a two-part paper, we develop and experimentally apply a method for tracking “slow” hidden variables causing drift in the parameters of a “fast” dynamical system. In part two of the paper, we develop a mathematical model of the experimental system, and make an analytical connection between the experimental method and the physics of the problem.

The idea of *time scale separation*, where a hidden process responsible for nonstationarity in a fast dynamical system evolves on a much slower time scale than the directly observable dynamics, is fundamental to this approach. A study of systems with this type of time scale separation is precisely what is required for the development of next-generation condition-based maintenance and failure prediction technology. For example, a collection of microcracks in a spinning shaft can be expected to grow slowly over many hundreds of thousands of typical vibrational time periods (e.g., shaft revolutions). The approach developed in this paper is not limited to material damage applications, but can be used for a general class of dynamical systems possessing the needed time scale separation. Possible applications include: the drifting out of alignment of machinery parts, corrosion processes in structural components, moisture accumulation in composite materials or electrical circuits, as well as cases involving material damage of various types.

In most cases, online real-time health monitoring and failure prediction for such systems requires assessment of the current state of damage in the system using only readily available vibration data: typically, a direct “damage sensor” is either not available, or requires the removal from service (or even destructive testing) of the machine in question. In many cases, even if a direct means of damage detection were available, it is not possible to add the required sensors because of cost or weight considerations. The approach presented here is designed to address these difficulties by using only readily available vibration data to track the slowly evolving failure process. At the same time, the abstract

formulation of the method means that it can in principle be applied to a wide variety of “damage” processes, to some degree independent of damage physics.

In the next section, a literature review is presented and used to frame a discussion of fundamental ideas underlying our approach. The tracking procedure based on phase space reconstruction is developed in Section 2. In Section 3 we apply the method to tracking a battery discharge process in an electromechanical experimental system using only strain gauge vibration data. In Section 4, we discuss the experimental results and compare our method to those based on attractor invariants. Finally, in Section 5 we present our conclusions.

2 Background

The main body of previous work relating to the effort presented here stems from studies relating to the development of condition based maintenance technologies, such as Fault Detection and Identification (FDI) theory. We should mention that most previous research, excluding studies dealing with fault severity assessment, have concentrated on detection of irregularities in the observable system. While the *detection* process estimates whether or not the system parameters or “fault indicators” have reached certain preset failure values, the *tracking* process as studied here, estimates in real-time the change in the slow state variables causing nonstationarity, a requirement for true prognostics.

The main idea behind FDI is to develop a procedure for obtaining feature vectors that are sensitive to the changes or failures in systems. There are several strategies for tackling this type of problem (see, for example, [1,2], for comparative studies). One basic approach is to use available signal processing techniques to develop a feature vector. We call these techniques heuristic, since they are not based on specific physics or analytical treatment of the problem. The early research was mainly concentrated on detecting changes in systems using time or frequency domain statistics (e.g., [3,4]). Later research considered techniques that carry both frequency and time domain information, such as wavelet transforms or Wigner-Ville distributions [5–9]. Other methods use such data classification schemes as principal component analysis,

Contributed by the Technical Committee on Vibrational and Sound for publication in the JOURNAL OF VIBRATION AND ACOUSTICS. Manuscript received July 2001; Revised Dec. 2001. Associate Editor M. I. Friswell.

neural networks or fuzzy logic (see, for example, [7,10]). For a study exploiting well-known characteristics of chaotic time series for detecting changes in a parameter, see [11].

The advantage of heuristic methods are that they are simple to implement and that they can work very well at times. However, a choice of feature vector that works well for one system may not work well for another, and there is no theoretical basis for predicting a priori, without the benefit of a good model or experiment, whether a certain choice of feature vector will work well or not. In addition, it is usually difficult to find a functional relation between the changes in system parameters and the changes in feature vectors.

Another, model-based approach to FDI provides several theoretical and practical advantages over simpler heuristic methods, typically at the expense of more time, effort or computation. For example, model-based approaches are fully general in that changes in any numbers of parameters can be detected, at least in principle, to the extent that the system's dynamics is affected by these parameter changes. In addition, if understanding of the system or its damage mechanisms improves, the model can still be used to address more subtle or sophisticated questions.

There is an extensive literature covering model-based FDI for linear dynamical systems (see, e.g., [12–14]). A good survey of the state of the art of nonlinear diagnostic observer design for FDI is given in [15]. A basic overview of the different approaches for fault diagnosis is given in [16]. The important advantage of the model based approach is that in many cases the changes in feature vectors can be related to changes in system parameters. However, to accomplish this, these methods require an explicit analytical model of the system (i.e., a known relationship between input and output). Unfortunately, in many cases the system's analytical model is unknown, or is hard to determine due to its complexity or inherently nonlinear behavior.

To overcome the problem of nonlinear analytical modeling imposed by methods based on the availability of physical models, many recent papers model nonlinear systems using genetic algorithms [17], or neural networks [10,18–20]. In this way it is possible to obtain a data-based model without determining one global physics-based nonlinear model. However, one loses the main advantage of global physics-based analytical models: the possibility to correlate faults or changes in model parameters with the feature vectors.

The method presented in this paper overcomes the main limitations of both heuristic and model-based methods by starting from an abstract formulation of the problem in state space. From the perspective of dynamical systems theory, we view a machine with evolving damage as a hierarchical dynamical system consisting of a “fast time,” directly observable, subsystem coupled to a “slow time” subsystem, with the form

$$\dot{\mathbf{x}} = \mathbf{f}(\mathbf{x}, \boldsymbol{\mu}(\boldsymbol{\phi}), t), \quad (1a)$$

$$\dot{\boldsymbol{\phi}} = \boldsymbol{\epsilon} \mathbf{g}(\mathbf{x}, \boldsymbol{\phi}, t), \quad (1b)$$

where $\mathbf{x} \in \mathbb{R}^n$ is the fast dynamic variable (directly observable state); $\boldsymbol{\phi} \in \mathbb{R}^m$ is the slow dynamic variable (“hidden” state); the parameter vector $\boldsymbol{\mu} \in \mathbb{R}^s$ is a function of $\boldsymbol{\phi}$; t is time; and $0 < \epsilon \ll 1$ defines the time scale separation between the fast dynamics and slow drift. If ϵ were exactly zero, then $\boldsymbol{\mu}(\boldsymbol{\phi}_0) = \boldsymbol{\mu}_0$ would be a constant vector of parameters in Eq. (1a); since ϵ is very small, we might consider Eq. (1a) to be a model for a system with slowly drifting parameters.

We assume that over intermediate time scales (times which are long compared to the fast dynamics but short compared to drift dynamics) the drift in the slow variable is negligible, and consider the fast subsystem to be approximately stationary (quasi-stationary). In the experimental procedure, the phase space of the fast subsystem Eq. (1a) is reconstructed using data recorded over intermediate time scales. Nonlinear predictive models are then estimated in the reconstructed phase space for the initial or refer-

ence system state. At future times, the difference between the actual dynamics and the dynamics predicted by the *reference model*, over a fixed short time interval, is used to quantify the slow drift in the fast dynamics.

3 Tracking Procedure

The essential idea for the tracking method may be motivated as follows. Consider a dynamical system, Eqs. (1), with a fixed hidden state vector $\boldsymbol{\phi}$ (i.e., for $\epsilon=0$). Now, imagine that the system starts at some initial point t_0 and $\mathbf{x}(t_0) = \mathbf{x}_0$ in the fast system's phase space. Then, at time $t_0 + t_p$ the state of the fast subsystem is

$$\mathbf{x}(t_0 + t_p) = \mathbf{X}(\mathbf{x}_0, t_0, t_p; \boldsymbol{\mu}(\boldsymbol{\phi})). \quad (2)$$

If we fix t_0 and \mathbf{x}_0 , then \mathbf{X} is purely a function of $\boldsymbol{\mu}(\boldsymbol{\phi})$ that describes a s -parameter surface in \mathbb{R}^n .

Now, imagine several experiments where the subsystem (Eq. 1a) is repeatedly started at the same initial point (t_0, \mathbf{x}_0) in the fast subsystem's phase space, but with slightly different values of $\boldsymbol{\phi}$ every time. In principle, $\mathbf{X}(\boldsymbol{\mu}(\boldsymbol{\phi}))$ can be evaluated for every $\boldsymbol{\phi}$, and given appropriate invertability (or, equivalently in this case, *observability*) conditions, one can construct mappings $\boldsymbol{\mu} = \mathbf{X}^{-1}(\mathbf{x}): \mathbb{R}^n \rightarrow \mathbb{R}^s$ or $\boldsymbol{\phi} = \mathbf{X}^{-1}(\mathbf{x}): \mathbb{R}^n \rightarrow \mathbb{R}^m$ required for true tracking. Therefore, if the function $X(\boldsymbol{\mu}(\boldsymbol{\phi}))$ can be determined experimentally, it can be used to determine changes in $\boldsymbol{\mu}(\boldsymbol{\phi})$ or in $\boldsymbol{\phi}$ provided the observability conditions are satisfied.

Now, let us consider the case of $\epsilon \neq 0$. For $0 < \epsilon \ll 1$, $\boldsymbol{\phi}$ cannot be treated as a parameter and, in this case, the complete state of the system Eqs. (1) is the direct product $(\mathbf{x}, \boldsymbol{\phi})$. We are interested in tracking changes in the slow variable $\boldsymbol{\phi}$ characterized by its average value over all $t \in t_D$, where t_D is the intermediate time interval and $t_p \ll t_D \ll 1/\epsilon$. For any $t_0 \in t_D$ we can write $\boldsymbol{\phi} = \boldsymbol{\phi}_0 + \mathcal{O}(\epsilon)$. Now, the state of the fast subsystem can be written as follows:

$$\begin{aligned} \mathbf{x}(t_0 + t_p; \epsilon) &= \mathbf{X}(\mathbf{x}_0, \boldsymbol{\mu}(\boldsymbol{\phi}), t_0, t_p), \\ &= \mathbf{X}(\mathbf{x}_0, t_0, t_p; \boldsymbol{\mu}(\boldsymbol{\phi}_R)) + \mathcal{O}(\epsilon), \\ &= \mathbf{X}(\mathbf{x}_0, t_0, t_p; \boldsymbol{\mu}(\boldsymbol{\phi}_R)) + \frac{\partial \mathbf{X}}{\partial \boldsymbol{\mu}} \frac{\partial \boldsymbol{\mu}}{\partial \boldsymbol{\phi}} (\boldsymbol{\phi}_0 - \boldsymbol{\phi}_R) \\ &\quad + \mathcal{O}(\|\boldsymbol{\phi}_0 - \boldsymbol{\phi}_R\|^2) + \mathcal{O}(\epsilon), \end{aligned} \quad (3)$$

where on the third line we have Taylor expanded the expression about $\boldsymbol{\phi}_R = \boldsymbol{\phi}(t_R)$, the reference value of the slow variable, for some reference time $t_0 = t_R$. Then, for fixed \mathbf{x}_0 , $\boldsymbol{\phi}_R$, and t_p , we define a *tracking function* as follows:

$$\begin{aligned} \mathbf{e} &\equiv \mathbf{X}(\mathbf{x}_0, \boldsymbol{\mu}(\boldsymbol{\phi}_0), t_0, t_p) - \mathbf{X}(\mathbf{x}_0, \boldsymbol{\mu}(\boldsymbol{\phi}_R), t_0, t_p), \\ &= \frac{\partial \mathbf{X}}{\partial \boldsymbol{\mu}} \frac{\partial \boldsymbol{\mu}}{\partial \boldsymbol{\phi}} (\boldsymbol{\phi}_0 - \boldsymbol{\phi}_R) + \mathcal{O}(\|\boldsymbol{\phi}_0 - \boldsymbol{\phi}_R\|^2) + \mathcal{O}(\epsilon), \end{aligned} \quad (4)$$

where the coefficient matrices in the Taylor expansion are evaluated at $\mathbf{x} = \mathbf{x}_0$ and $\boldsymbol{\phi} = \boldsymbol{\phi}_R$.

Now, it is clear that the observability condition is that the matrix $(\partial \mathbf{X} / \partial \boldsymbol{\mu})(\partial \boldsymbol{\mu} / \partial \boldsymbol{\phi})$ must have maximal rank. That is, we should have $n > s > m$, in addition to $\text{Range}(\partial \mathbf{X} / \partial \boldsymbol{\mu}) \subset \mathbb{R}^n$ and $\text{Range}(\partial \boldsymbol{\mu} / \partial \boldsymbol{\phi}) \subset \mathbb{R}^s$ having dimensions s and m , respectively.

Assuming that the linear operator in the first term of the Taylor expansion Eq. (4) has maximal rank, we expect the output of the tracking function to be an affine transformation of the drifting variable (*linear observability*):

$$\mathbf{e} = \mathbf{C}(\mathbf{x}_0, t_0, t_p) \boldsymbol{\phi}_0 + \mathbf{c}(\mathbf{x}_0, t_0, t_p, \epsilon), \quad (5)$$

where, $\mathbf{C} = (\partial \mathbf{X} / \partial \boldsymbol{\mu})(\partial \boldsymbol{\mu} / \partial \boldsymbol{\phi})$ is an $n \times m$ matrix, and $\mathbf{c} = -(\partial \mathbf{X} / \partial \boldsymbol{\mu})(\partial \boldsymbol{\mu} / \partial \boldsymbol{\phi}) \boldsymbol{\phi}_R + \mathcal{O}(\|\boldsymbol{\phi}_0 - \boldsymbol{\phi}_R\|^2) + \mathcal{O}(\epsilon)$ is an $n \times 1$ vector; all terms are evaluated using $\mathbf{x} = \mathbf{x}_0$ and $\boldsymbol{\phi} = \boldsymbol{\phi}_R$. We remark that even when linear observability fails, higher order observability may in many cases be possible.

In an experimental context, however, the procedure illustrated above is prone to errors. It is usually impossible to repeatedly start the system from the same initial condition. Furthermore, the observability conditions clearly depend on \mathbf{x}_0 , t_0 , and t_p , and so we might attempt to somehow use many values of \mathbf{x}_0 and/or t_0 and/or t_p to deal with this repeatability problem as well as to increase the robustness of the method. Such an approach, where the behaviors of two systems are compared for many different values of starting times, initial conditions and observation times, is philosophically similar to a model-based approach to tracking.

The best way to examine the tracking function e over many different values of \mathbf{x}_0 and/or t_0 and/or t_p depends on the system. For example, in linear autonomous systems, a quantity commonly used to track changes in system parameters is a suitable frequency response function (FRF). Since the FRF is equivalent to the response of the system to a unit impulsive input, in such an approach one essentially fixes \mathbf{x}_0 and examines the response for many (in fact, all) values of t_p . In contrast, if for example, the system is chaotic in its reference state (and hence nonlinear), then averaging over many values of \mathbf{x}_0 is easily possible simply by following the fast system's trajectory as it explores the phase space. This is essentially the approach followed here, as discussed in greater detail in Section 3.2.

To actually calculate the tracking function \mathbf{e} , we need to know how the fast subsystem evolves over the time interval t_p for the current value of ϕ_0 , as well as how the subsystem *would have* evolved for the reference value of ϕ_R , both evolving from the same initial condition x_0 . Since the system's fast time behavior for the current hidden subsystem state characterized by ϕ_0 is directly measurable (i.e., we can reconstruct the fast dynamics using a sensor measurement from the fast system), the strategy used in this paper is to compare it to the predictions of a *reference model* describing the fast subsystem behavior for $\phi = \phi_R + \mathcal{O}(\epsilon)$.

3.1 Reference Model Construction. The reference model should predict how the fast subsystem evolves starting from any point \mathbf{x}_0 in the reference phase space. Since the fast subsystem is nonstationary over long time scales $t = \mathcal{O}(1/\epsilon)$, it might undergo many bifurcations in its behavior over the course of any given experiment. Hence, the region of the phase space over which the reference model is valid should be large enough to encompass all expected orbits of the fast subsystem.

One way to construct a reference model valid over a given portion of phase space is to repeatedly start the reference subsystem from randomly generated initial conditions that adequately cover the region of interest (e.g., by stochastic interrogation, as in [21,22]). However, we do not consider this approach here. By design, the system considered in this paper is chaotic in its reference state: since, as is well known, chaotic trajectories explore a fairly large region of phase space, they automatically provide a convenient source of data for nonlinear state space modeling. We emphasize, however, that this use of chaos to obtain the reconstructed reference phase space for modeling should be viewed as an experimental and theoretical convenience: in principle, the same tracking procedure described in the following sections could be applied to arbitrary global system behaviors (including multiple coexisting periodic orbits and random excitation). However, this would be accompanied by an increase in the difficulty and complexity of the data acquisition task.

We assume that the effective dimensionality of the system (i.e., the minimum number of active degrees of freedom needed to represent the dynamics) does not increase during the entire time of observation. We also assume that the phase space trajectories observed for all future system conditions stay predominantly within the region for which the reference model is valid. The basic form of the tracking procedure described here will fail if the change in the slow subsystem causes the observed dynamics to shift out of this reference domain. In such cases, the reference model would need to be established afresh for adequate tracking.

We measure a scalar time series corresponding to some C^2

function of the fast variables of the system Eq. (1a), sampled at equal time intervals. Using delay reconstruction [23,24] the scalar time series $\{x(n)\}_{n=1}^M$ is used to reconstruct a phase space of appropriate dimension (say, d) for the system. In this reconstructed phase space the scalar time series is converted to a series of vectors $\mathbf{y}^T(n) = (x(n), x(n+\tau), \dots, x(n+(d-1)\tau)) \in \mathbb{R}^d$, where τ is a suitability delay parameter. Embedding parameters τ and d are determined using the first minimum of the average mutual information [25] and false nearest neighbors [26] methods, respectively.

The reconstructed state vectors are governed by an as yet undetermined map of the form $\mathbf{y}(n+1) = \mathbf{P}(\mathbf{y}(n); \phi)$. The observation period t_p discussed earlier now corresponds to picking an integer k . We examine the k^{th} iterate of the map \mathbf{P} , i.e.,

$$\mathbf{y}(n+k) = \mathbf{P}^k(\mathbf{y}(n); \phi). \quad (6)$$

Working in the global reconstructed phase space of the dynamical system, local models which show how neighborhoods about each data point are mapped forward in time can be estimated. The simplest such model is a *local linear* model relating the state at time n , $\mathbf{y}(n)$ to the state $\mathbf{y}(n+k)$ at time $n+k$:

$$\mathbf{y}(n+k) = \mathbf{A}_n \mathbf{y}(n) + \mathbf{a}_n = \mathbf{B}_n \hat{\mathbf{y}}(n), \quad (7)$$

where the model parameter matrix \mathbf{A}_n and a parameter vector \mathbf{a}_n provide local approximations of \mathbf{P}^k , and are determined by regression at each point in the data set, and where

$$\hat{\mathbf{y}}(n) = [\mathbf{y}^T(n), 1]^T, \quad \text{and} \quad \mathbf{B}_n = [\mathbf{A}_n | \mathbf{a}_n] = [b_{pq}^n]. \quad (8)$$

Basing our model on N nearest neighbors ($\mathbf{y}^r(l)$, $r=1, \dots, N$) of the point of interest ($\mathbf{y}(l)$) we can determine the optimum model parameters by minimizing

$$\begin{aligned} \mu_k^2 &= \sum_{r=1}^N w^r(l) |\mathbf{y}^r(l+k) - \mathbf{B}_l \mathbf{y}^r(l)|^2 \\ &= \sum_{r=1}^N w^r(l) \sum_{n=1}^d \left(\mathbf{y}_n^r(l+k) - \sum_{m=1}^{d+1} b_{nm}^l \hat{\mathbf{y}}_m^r(l) \right)^2, \end{aligned}$$

where $w^r(l)$ is some weighting function. Minimizing μ_k^2 with respect to each b_{pq}^l (l is fixed) we obtain

$$\sum_{r=1}^N w^r(l) \mathbf{y}_p^r(l+k) \hat{\mathbf{y}}_q^r(l) = \sum_{r=1}^N w^r(l) \sum_{m=1}^{d+1} b_{pm}^l \hat{\mathbf{y}}_m^r(l) \hat{\mathbf{y}}_q^r(l). \quad (9)$$

It is then easy to show that

$$\mathbf{B}_l = \mathbf{Y}_{l+k} (\mathbf{W} \hat{\mathbf{Y}}_l)^T (\hat{\mathbf{Y}}_l (\mathbf{W} \hat{\mathbf{Y}}_l)^T)^{-1}, \quad (10)$$

where

$$\mathbf{Y}_l = [\mathbf{y}^1(l) \mathbf{y}^2(l) \dots \mathbf{y}^N(l)], \quad (11a)$$

$$\mathbf{W} \hat{\mathbf{Y}}_l = [w^1(l) \hat{\mathbf{y}}^1(l) w^2(l) \hat{\mathbf{y}}^2(l) \dots w^N(l) \hat{\mathbf{y}}^N(l)], \quad (11b)$$

$$\hat{\mathbf{Y}}_l = [\hat{\mathbf{y}}^1(l) \hat{\mathbf{y}}^2(l) \dots \hat{\mathbf{y}}^N(l)]. \quad (11c)$$

3.2 Tracking Function and Tracking Metric Estimation.

The basic ideas are shown schematically in Fig. 1. First, a large reference data set is collected and used to reconstruct the reference phase space (reference trajectories are shown in gray). Then, a sufficiently large number of initial points $\mathbf{y}(l)$ ($l=1, 2, \dots$) is obtained, together with the corresponding points after k steps, $\mathbf{y}(l+k)$, for the "changed" system. The N points in the reference set that are nearest neighbors of each point $\mathbf{y}(l)$ are looked up, along with the corresponding N reference data points k steps later. Based on these points we build the reference model for each point $\mathbf{y}(l)$ as described in the previous section. In the reference system the same initial points $\mathbf{y}(l)$ would have been mapped to points $\mathbf{y}^R(l+k)$. Since we have an imperfect reference model, it actually maps these same points to some other points $\mathbf{y}^M(l+k)$.

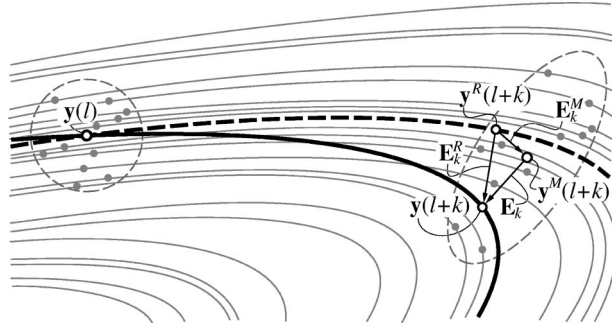


Fig. 1 Schematic drawing illustrating the basic idea behind tracking function estimation. Trajectories of the reference system in phase space are shown in gray. The solid black line represents a measured trajectory of the perturbed system, passing through $\mathbf{y}(l)$ and the dashed gray line represents where a trajectory would have gone in the reference system, if starting from the same point $\mathbf{y}(l)$.

We introduce the following “error” vectors (for clarity, the dependence of the \mathbf{E} 's on l is suppressed in the figure):

$$\mathbf{E}_k^R(l) = \mathbf{y}(l+k) - \mathbf{y}^R(l+k), \quad \text{the true error,} \quad (12a)$$

$$\mathbf{E}_k(l) = \mathbf{y}(l+k) - \mathbf{y}^M(l+k), \quad \text{the estimated error,} \quad (12b)$$

$$\mathbf{E}_k^M(l) = \mathbf{y}^M(l+k) - \mathbf{y}^R(l+k) \quad \text{the modeling error.} \quad (12c)$$

The tracking function (Eq. (4)) for initial point $\mathbf{y}(l)$ in the reconstructed phase space can then be written as

$$\mathbf{e}_k(l) = \mathbf{P}^k(\mathbf{y}(l), \boldsymbol{\phi}_0) - \mathbf{P}^k(\mathbf{y}(l), \boldsymbol{\phi}_R) = \mathbf{E}_k^R(l) = \mathbf{E}_k(l) + \mathcal{O}(\mathbf{E}_k^M(l)). \quad (13)$$

Note that $\mathbf{e}_k(l)$ is equal to the true error vector $\mathbf{E}_k^R(l)$, but since we cannot determine it directly, we use the estimated error vector $\mathbf{E}_k(l)$ in its place. In general, this is justified if the modeling error $\mathbf{E}_k^M(l)$ is small compared to the true error $\mathbf{E}_k^R(l)$.

Consideration of Eq. (13) shows that there are two main sources of fluctuation in the empirical tracking function that are not related to changes in $\boldsymbol{\phi}$. First, and most obviously, the $\mathcal{O}(\mathbf{E}_k^M(l))$ term corresponds to fluctuations caused by changes in the model accuracy from point to point. Second, Eq. (13) was derived holding the initial point \mathbf{x}_0 in the reconstructed phase space fixed (as indicated by the index l): however, as shown by Eq. (5), the mapping relating changes in $\boldsymbol{\phi}$ to changes in \mathbf{e} will in general depend on \mathbf{x}_0 . We compensate for both sources of fluctuation by using suitable averages, as described below. This approach has the added benefit of using all of the data available within one data record.

Using the local linear models, from a scalar time series collected experimentally for the slightly changed system, the error vector $\mathbf{E}_k(l)$ of Eq. (12) can be calculated for a large number of points that lie on the trajectory of the changed system. Then, a single scalar measure for the drift, or *tracking metric*, can be obtained from the set of all values of the estimated tracking function evaluated for all $t_0 \in t_D$. Specifically, we consider the root mean square (RMS) magnitude of \mathbf{e}_k as defined by:

$$e_k^2 = \langle \mathbf{e}_k^T \mathbf{e}_k \rangle \approx \frac{\sum_{l=1}^M q(l) \|\mathbf{E}_k(l)\|^2}{\sum_{l=1}^M q(l)}, \quad (14)$$

where $\langle \rangle$ denotes a weighted average over different \mathbf{x}_0 ($\forall t_0 \in t_D$), \mathbf{a}^T denotes the transpose of \mathbf{a} , and $q(l)$ is an appropriate weighting function.

As mentioned earlier, the use of $\mathbf{E}_k(l)$ as an estimate of $\mathbf{e}_k(l)$ is justified only if the modeling error $\mathbf{E}_k^M(l)$ is small compared to the true error $\mathbf{E}_k^R(l)$. Hence, the weighting function $q(l)$ is selected so that the points with more accurate local fits are weighted more

than the points with less accurate fits. Note that the smaller the region in which the N nearest neighboring points lie, the more accurate the fitted linear map is expected to be. This would be equivalent to saying that local models are more accurate for the region that have a higher probability density of data points in the reference phase space. Therefore, a good choice for the weighting would be $q(l) \propto f(l)$, where $f(l)$ is the reference data probability density near $\mathbf{y}(l)$. Thus the weighting used in the tracking metric is,

$$q(l) = \frac{1}{r_l^{d_p}}. \quad (15)$$

Here, r_l is the distance from the point $\mathbf{y}(l)$ to the farthest of all N nearest neighbors and d_p is the estimated *pointwise dimension* of the data in the reference phase space (see [27], pg. 86). The fact that the expected value of this weighting is proportional to the density of reference data points follows directly from the definition of d_p .

Note that the above choice for $q(l)$ means that points on the *current* trajectory that lie in a region of the reconstructed reference phase space where no *reference* data is available are weighted very lightly during the e_k calculation. Therefore, if we have large data sets and most of the changed trajectory lies inside the reconstructed reference phase space we can still accurately estimate e_k , even though a few of the points on the current trajectory are outside of the region in the original phase space occupied by the reference data.

The weighted average described by Eqs. (14) and (15) compensates for model accuracy fluctuations from point to point *within* each data record. However, the statistic (tracking metric) of Eq. (14) will still typically fluctuate from *record to record* because of fluctuations in the population of initial conditions used to generate e_k . This is compensated for by taking a moving average of the tracking metric, \bar{e}_k , over many data records: it is most convenient to discuss the details of this step by examining the effect on actual experimental data, which we do in the next section.

If there is more than one drifting parameter, then a more sophisticated use of the tracking function \mathbf{e}_k will be needed. Obviously, the scalar tracker would not be enough to unambiguously describe several drifting slow state variables simultaneously. However, we show later that the single scalar measure described here does a reasonable job of resolving small changes in a single drifting state variable.

4 Experimental Application to an Electromechanical System

We now apply the tracking procedure to an electromechanical system in the laboratory (see Fig. 2 for a schematic diagram). The pendulum-type oscillator consists of a flexible steel beam with additional stiffening elements added to constrain the system to one degree of freedom over the frequency range of interest (< 50 Hz). This system is a modification of the magneto-elastic oscillator of [28], as studied in [21,22] and [29]. Extra stiffness to the system is added in the form of steel bars (each 192.1 mm \times 5.2 mm \times 12.8 mm) along the length of the thin steel beam (209.6 mm \times 0.7 mm \times 12.8 mm). The steel bars are attached to each side of the thin steel beam, away from the clamped end, using bolts. The top of the beam is left clear to act as a hinge, and also has an attached strain gauge, allowing the beam's position to be determined.

The nonlinear potential at the beam tip is realized using a permanent magnet for one well and permanent/electromagnet stack for the other. The oscillator is mounted on an electro-mechanical shaker, which provides a harmonic displacement excitation to the system. The signal from the strain gauge is amplified, digitized (using a 12-bit A/D converter) and stored in a computer along with the signal from the coil of the electromagnet. The electro-

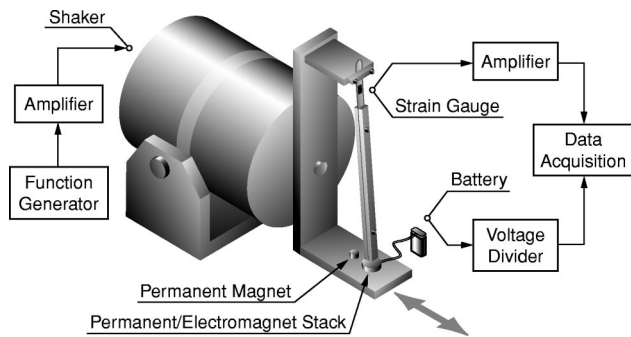


Fig. 2 Schematic diagram of the experiment with the two-well electromechanical oscillator

magnetic modification to the standard realization of the nonlinear potential was chosen since it allowed us to introduce a controlled drift process in one of the energy wells.

Power to the electromagnet was supplied by a 9 V battery which was allowed to discharge completely during each experiment. The open circuit battery voltage played the role of a hidden drift state variable. To determine the effect of the battery on the basic mechanical properties of the system, natural frequencies in the potential energy wells were determined from frequency response function estimates. The natural frequency in the permanent magnet well was 7.45 ± 0.04 Hz, and in the permanent/electromagnet well it changed from 8.83 ± 0.04 Hz to 8.56 ± 0.04 Hz as the battery completely discharged. This observed 3.05 percent change in the frequency corresponds approximately to a 6 percent change in effective stiffness in the electromagnet energy well as the battery discharges.

4.1 Tracking the Discharge of a “Hidden” Battery. Using a wave form generator, a forcing frequency (6.3 Hz) and suitable forcing amplitude were selected to ensure that the system exhibited chaotic behavior during at least the beginning of the experiment. The data collection was started with a fresh 9 V battery and continued for just under seven hours until complete discharge of the battery. Strain gauge and electromagnet voltage data was collected with a 100 Hz sampling frequency, and a total of 2.5×10^6 data points were recorded over the course of the entire experiment. The uniformity of power spectra taken during the experiment (see Fig. 3, left) shows that the system was in fact nominally chaotic throughout most of the experiment, and that the basic characteristics of the chaotic motions did not appear to undergo any drastic changes. However, the situation was not quite as

simple as the power spectra suggest. First of all, since the system is not stationary, it cannot strictly speaking be considered chaotic at any time, since it is never truly at steady state. More importantly however, even if one considers the system to be approximately stationary in any one data record (as we do), numerous bifurcations through windows of periodic behavior were observed over the range of stiffness traversed by the system as the battery discharged (see Fig. 3, right).

Average mutual information and false nearest neighbors were used to select a delay τ of five sampling time steps, and an embedding dimension $d=5$. We remark that this embedding dimension is consistent with a forced, single degree-of-freedom system. The first 2^{14} data points of the entire data set were used for the reference data. After phase space reconstruction, the reference data was partitioned in a $k-d$ tree [30] for fast local linear model construction. The average point-wise dimension of the reference data set was found to be 2.82, and 16 nearest neighbors were used for local linear modeling.

For the tracking metric we picked e_5 due to the fact that $\tau=5$. Given the uniform embedding used here, new information is added only in the last coordinate for points in the reconstructed space that are τ time units apart (the other coordinates simply shift to the left). This means that the short-time prediction is much simpler since only one component of the next state needs to be estimated at each step.

We used data records each of $M=2^{12}$ points to calculate e_5 . In particular, the entire reconstructed data set was divided into consecutive records of size M , and within each record we calculated e_5 (from Eq. 14) using all M data points. Then \bar{e}_5 , and the standard deviation in its estimate, was calculated using a moving average of the values of e_5 determined from N_R consecutive M -point records, for $N_R=10, 20$, and 40.

We have at the present time spent little effort optimizing the code for speed. Nevertheless, the current implementation can be used for many real-time on-line applications. The reference model preparation (essentially $k-d$ tree partitioning) took about 36 seconds on a Pentium III 600 MHz laptop system using Matlab 6, and the calculation of each e_5 took about 2 seconds. Simply compiling the code in C or Fortran would significantly speed up the process, and further optimizations are possible and will be taken up in future efforts.

4.2 Discussion of the Results. A plot of raw (unscaled) results showing the local mean reference model prediction error, \bar{e}_5 , versus the local mean of the battery voltage, is shown in Fig. 4 (left). Local means correspond to moving averages over $N_R=10$ consecutive M -point data records. Black dots show \bar{e}_5 , and the gray background represents \pm one standard deviation. The

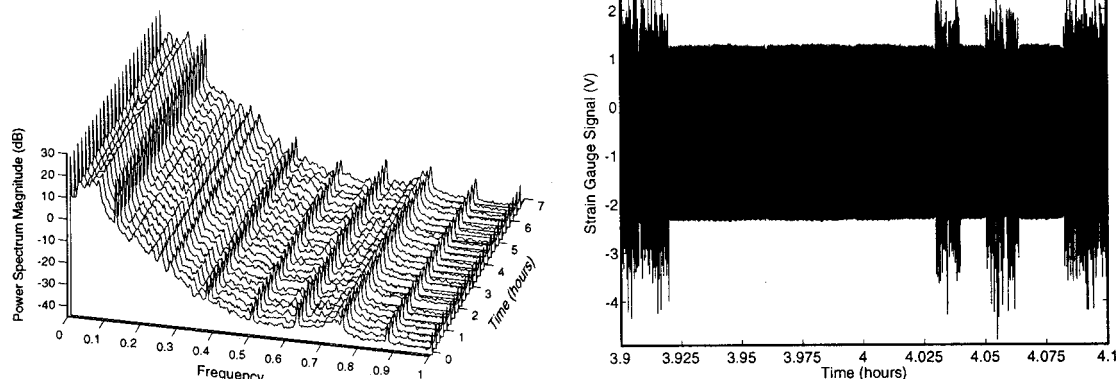


Fig. 3 Power spectra taken throughout the experiment (left). Passages through periodic windows occurring during the experimental run (right). See text for further discussion.

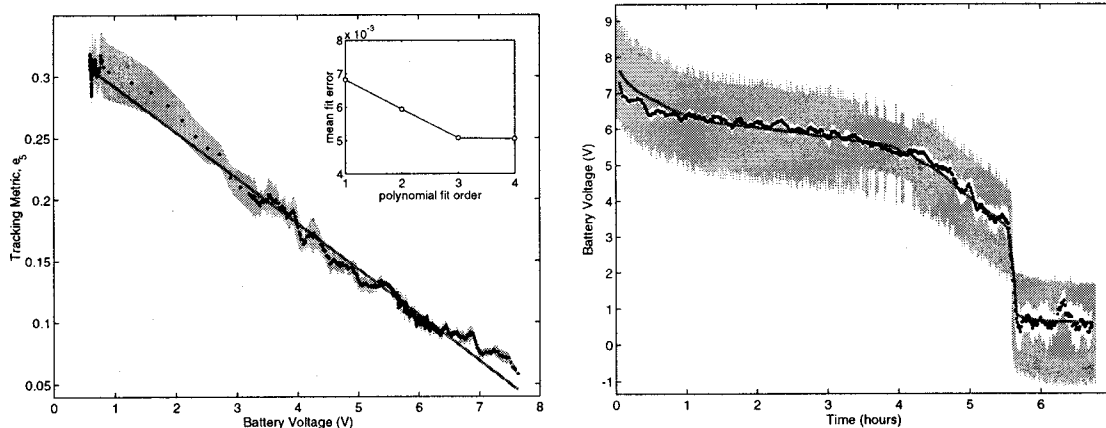


Fig. 4 Experimental tracking results: (left) plot of unscaled tracking metric \bar{e}_5 vs. the battery voltage; (right) scaled battery voltage vs. time. In both figures, black dots show the moving average of tracking metric over ten data records, and the gray background represents \pm one standard deviation of the mean. In the right figure, the dark gray gives the outline of the actual (unaveraged) battery voltage, and the solid gray line is the corresponding local average in one data record.

subplot in the top right corner in the left plot of Fig. 4 shows the mean error of a polynomial fit to \bar{e}_5 as a function of the battery voltage, versus the corresponding order of the fit. The subplot demonstrates that the inclusion of higher order terms does not significantly improve the fit. Therefore, a strong linear relationship is evident between the tracking metric and the battery voltage (the gray line shows a linear fit to the data). Thus, the open circuit battery voltage is linearly related to \bar{e}_5 , as suggested by Eq. (5).

In Fig. 4 (right), the tracking metric is plotted, scaled using the linear fit from Fig. 4 (left). In other words, the linear fit to \bar{e}_5 provides the affine transformation Eq. (5), as discussed in Section 2. In the figure, the scaled drift tracker \bar{e}_5 (black dots) is plotted over the measured battery voltage (dark gray lines). The large oscillation in the measured battery voltage is caused by inductance changes as the vibrating beam passes over the top of the electromagnet. However, the local average (in each data record) of the measured battery voltage (solid thick gray line) corresponds to the open circuit battery voltage and is the true hidden state.

From Fig. 4, we can clearly see that the variation in the metric is certainly due to the change in the drifting variable, and is not an artifact of our calculation. Thus, we have experimentally constructed a mapping between the tracking metric based on the reconstructed fast state variable (using the fast-time strain signal), and the drifting hidden state variable (the battery state). Specifically, a one-to-one mapping (in fact, in this case, a *linear* mapping) exists between the tracking function and local time average of the drifting variable (local mean battery voltage).

Note that \bar{e}_5 's tracking performance is relatively poor at the initial stage (i.e., for relatively small net drift corresponding to relatively small initial changes in the battery voltage). This is caused by the unavoidable imperfections in the reference model. As discussed in Section 3.2 and illustrated by Fig. 1, one cannot clearly distinguish changes in the slow subsystem state variable that are smaller than the inherent modeling error (Eq. (12c)). Therefore, the tracker is expected to have an initial "settling in" period close to the initial (reference) value of the slow subsystem state variable.

In Fig. 5, the effect of varying the number of consecutive records used to calculate the moving average \bar{e}_5 is shown. Note that the time needed to acquire data for one $M=2^{12}$ point record is about 41 seconds at 100 Hz. Thus, $N_R=10, 20,$ and 40 equates to a moving average over about 2, 4, and 8 percent, respectively, of the total time of the experiment. An automatic, objective criterion for selecting the best value of N_R to use in the moving average is not currently available, and the user must proceed by trial

and error and with due regard to the requirements of a given application. However, it is clear from the figures that the selection of the moving average affects only the local fluctuations in, and not the general qualitative features of, the tracking metric.

As explained in Section 3.2, the moving average \bar{e}_k is needed to compensate for fluctuations in the tracking metric caused by changes, from record to record, in the population of initial conditions used to compute the tracking function. In general, N_R must be selected large enough so that these sample-induced fluctuations are minimized, but small enough to allow actual changes in ϕ to be usefully tracked. In nonlinear systems, such fluctuations can be significant since, during the course of any experiment, the system may pass through many bifurcations causing the population of points available to calculate e_k in any record to change significantly.

It must be emphasized, however, that these particular fluctuations (and hence the need for the local averages) are *not* the result of changes in the local maps or model inaccuracies: as discussed in Section 3, the short time prediction error is theoretically *insensitive* to passages through bifurcations, which is why we have used it as the basis for the tracking algorithm. The benefits of this characteristic of the method are demonstrated in more detail in the next section.

4.3 Comparison to Methods Based on Asymptotic Invariants.

It is worth comparing the results using the methods of this paper with approaches that attempt to monitor damage using the asymptotic invariants of a chaotic attractor. For example, in Golnaraghi et al. [31], estimates of the correlation dimension and Lyapunov exponents are used to detect changes in the "chaotic signature" of the vibration signal from a damaged gearbox. They were able to observe variations in the Lyapunov exponents and correlation dimension after a crack was filed in a gear. Other applications of correlation dimension to damage monitoring are described in [32–34] for systems with clearance, gearbox, and rolling element condition monitoring, respectively.

To investigate how long-time asymptotic quantities compare with the tracking results using our algorithm, we have calculated the correlation dimension (d_c) and largest short time Lyapunov exponent (λ_1) using the same strain gauge data as for our \bar{e}_5 calculation. Both d_c and λ_1 were obtained using the algorithm of [35]. Figure 6 depicts the results of these calculations, with circles showing the record mean values.

While it is clear that such asymptotic invariants can be used to detect *changes* in a system caused by damage, it is also clear that

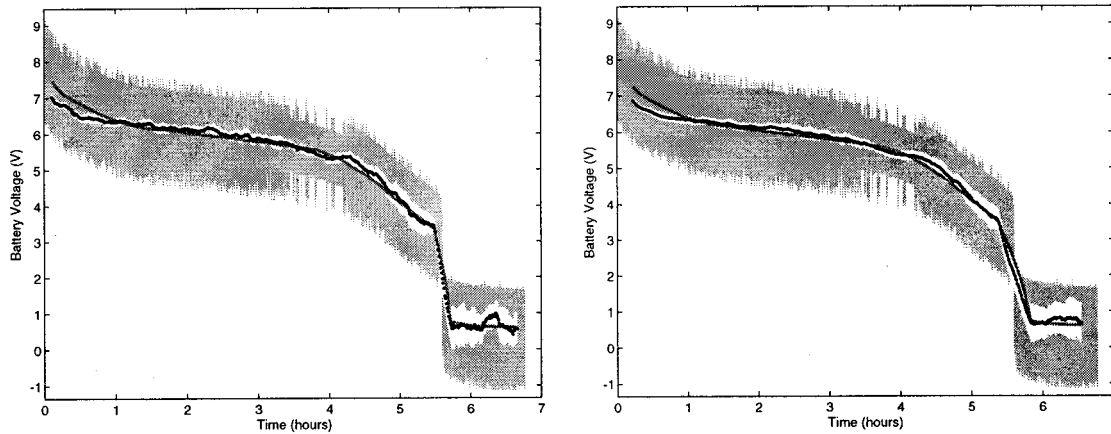


Fig. 5 Additional tracking results showing the effect of changing N_R , the number of consecutive records used for the moving average \bar{e}_5 : (left) $N_R=20$; (right) $N_R=40$. Plot details are the same as in Fig. 4. As can be seen by comparison with Fig. 4, the different values of N_R affect only the local fluctuations of the tracking, not the general trend.

they are unsuitable for actual damage *tracking*, since they do not vary monotonically with the hidden variable. This is a consequence of the fact that the asymptotic invariants do not vary smoothly with system parameters as the system passes through various bifurcations during the experiments. For example, in Fig. 6 both asymptotic measures were able to detect the passage through periodic windows at about 5.5 V when the correlation dimension approaches one and the largest Lyapunov exponent tends to zero, however, neither statistic can be used to establish a one-to-one mapping with the battery voltage.

In contrast, the average short time reference model prediction error (tracking metric) \bar{e}_5 is *not sensitive to bifurcations*, and continues to monotonically track the hidden variable even when the system is repeatedly switching between chaotic and periodic behaviors. Even though the initially chaotic state of the system was used for the reference model, it performs well even as the system passes through periodic windows, as seen in Figs. 4 and 5.

5 Conclusions

Motivated by the need to track slowly evolving hidden damage in machinery, in this paper we have presented a new method for tracking hidden processes responsible for nonstationarity in an observed system. A tracking metric for the hidden variable is computed from the short time prediction error of a reference model, and is constructed using only directly observable data from the

fast system. Given its abstract dynamical systems formulation, the method is independent of the damage physics in any given problem, and is therefore applicable to a variety of systems with suitable time scale separation.

After describing the method, it was successfully applied to the problem of tracking the discharge, over about seven hours, of a “hidden” battery in a nonlinear oscillator using only strain gauge vibration data sampled at 100 Hz. The connection between the tracking metric and the battery voltage was demonstrated explicitly by independently measuring and recording the battery terminal voltage. It was shown that for small changes in the battery-powered restoring force (six percent total change in stiffness) the tracking metric was in a linear, one-to-one relationship with the drifting variable, as suggested by the theory. In contrast, asymptotic attractor invariants (specifically, the largest Lyapunov exponent and the correlation dimension) were shown to vary in a nonsmooth fashion with the hidden variable, and therefore are not suitable for tracking.

In the next part of this paper, a physics-based mathematical model of the experimental system is derived. Numerical experiments are then used to validate the method, and provide additional insight into its physical meaning.

Acknowledgments

This work was supported by the Office of Naval Research MURI on Integrated Predictive Diagnostics, Grant #N0014-95-0461.

References

- [1] Qu, L., Xie, A., and Li, X., 1993, “Study and Performance Evaluation of Some Nonlinear Diagnostic Methods for Large Rotating Machinery,” *Mech. Mach. Theory*, **28**(5), pp. 699–713.
- [2] Ma, J., and Li, C. J., 1995, “On Gear Localized Defect Detection by Demodulation of Vibrations—A Comparison Study,” E. Kannatey-Asibu, J., ed., *Proc. of Symp. on Mechatronics for Manufacturing in ASME International Mechanical Engineering Congress and Exposition*, MED-2-1, pp. 565–576.
- [3] McFadden, P. D., and Smith, J. D., 1985, “A Signal Processing Technique for Detecting Local Defects in a Gear From the Signal Averaging of Vibration,” *Proc. Inst. Mech. Eng., Part C: Mech. Eng. Sci.*, **199**(c4), ImechE-1985.
- [4] Robert, T. S., and Lawrence, J. M., 1986, “Detection, Diagnosis and Prognosis of Rotating Machinery,” *Proc. of the 41st Meeting of the Mech. Failures Prevention Group*, Naval Air Test Center, Patuxent River, Maryland.
- [5] McFadden, P. D., and Wang, W. J., 1993, “Early Detection of Gear Failure by Vibration Analysis—I. Calculation of the Time-Frequency Distribution,” *Mech. Syst. Signal Process.*, **37**(3), pp. 193–201.
- [6] Liu, B., Ling, S., and Meng, Q., 1997, “Machinery Diagnosis Based on Wavelet Packets,” *J. Vib. Control*, **3**, pp. 5–17.
- [7] Baydar, N. Ball, A., and Kruger, U., 1999, “Detection of Incipient Tooth Defect in Helical Gears Using Principal Components,” Starr, A. G., Leung, A.

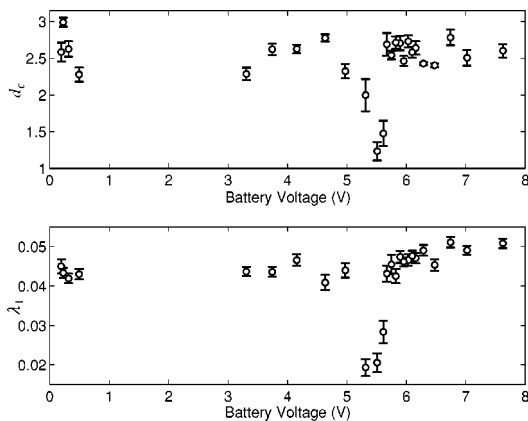


Fig. 6 The correlation dimension (d_c) and largest short time Lyapunov exponent (λ_1) vs. the battery voltage. See the discussion in text.

- Y. T., Wright, J. R., and Sandoz, D. J., eds. *Integrating Dynamics, Condition Monitoring and Control for the 21st Century*, A. A. Balkema, Rotterdam, Brookfield, pp. 93–100.
- [8] Staszewski, W. J., Worden, K., and Tomlinson, G. R., 1997, "Time-frequency Analysis in Gearbox Fault Detection Using the Wigner-Ville Distribution and Pattern Recognition," *Mech. Syst. Signal Process.*, **11**(5), pp. 673–692.
- [9] Staszewski, W. J., and Tomlinson, G. R., 1994, "Application of the Wavelet Transform to Fault Detection in a Spur Gear," *Mech. Syst. Signal Process.*, **8**(3), pp. 289–307.
- [10] Kim, T., and Li, C. J., 1995, "Feedforward Neural Networks for Fault Diagnosis and Severity Assessment of a Screw Compressor," *Mech. Syst. Signal Process.*, **9**(5), pp. 485–496.
- [11] Chancellor, R. S., Alexander, R., and Noah, S., 1996, "Detecting Parameter Changes Using Experimental Nonlinear Dynamics and Chaos," *ASME J. Vib. Acoust.*, **118**, pp. 375–383.
- [12] Isermann, R., 1984, "Process Fault Detection Based on Modeling and Estimation Methods—A Survey," *Automatica*, **20**(4), pp. 387–404.
- [13] Patton, R., Frank, P., and Clark, P., 1989, *Fault Diagnosis in Dynamical Systems: Theory and Application*, Princeton Hall International (UK) Ltd.
- [14] Gertler, J., 1988, "Survey of Model-Based Failure Detection and Isolation in Complex Plants," *IEEE Control Syst. Mag.*, **8**(6), pp. 3–11.
- [15] Nijmeijer, H., and Fossen, T. I., 1999, "New Directions in Nonlinear Observer Design," *Lecture Notes in Control and Information Sciences*, Springer-Verlag, London, pp. 351–466.
- [16] Ashton, S. A., and Shields, D. N., 1999, "Fault Detection Observer for a Class of Nonlinear Systems," Nijmeijer, H., and Fossen, T. I., eds., *New Directions in Nonlinear Observer Design, Lecture Notes in Control and Information Sciences*, Springer-Verlag, London, pp. 353–373.
- [17] Jeon, Y. C., and Li, C. J., 1995, "Non-linear ARX Model Based Kullback Index for Fault Detection of a Screw Compressor," *Mech. Syst. Signal Process.*, **9**(4), pp. 341–358.
- [18] McGhee, J., Henderson, I. A., and Baird, A., 1997, "Neural Networks Applied for the Identification and Fault Diagnosis of Process Valves and Actuators, J. of Int. Measr. Confederation," **20**(4), pp. 267–275.
- [19] Alessandri, A., and Parisini, T., 1997, "Model-Based Fault Diagnosis Using Nonlinear Estimators: A Neural Approach," *Proceedings of the American Control Conference*, **2**, pp. 903–907.
- [20] Li, C. J., and Fan, Y., 1997, "Recurrent Neural Networks for Fault Diagnosis and Severity Assessment of a Screw Compressor," *DSC ASME Dynamic Systems & Control Division*, **61**, pp. 257–264.
- [21] Cusumano, J. P., and Kimble, B., 1995, "A Stochastic Interrogation Method for Experimental Measurements of Global Dynamics and Basic Evolution: Application to a Two-Well Oscillator," *Nonlinear Dyn.*, **8**, pp. 213–235.
- [22] Kimble, B. W., and Cusumano, J. P., 1996, "Theoretical and Numerical Validation of the Stochastic Interrogation Experimental Method," *J. Vib. Control*, **2**, pp. 323–348.
- [23] Takens, F., 1981, "Detecting Strange Attractor in Turbulence," Rand, D. A., and Young, L. S., eds. *Dynamical Systems and Turbulence, Warwick, Springer Lecture Notes in Mathematics*, Springer-Verlag, Berlin, pp. 336–381.
- [24] Sauer, T., Yorke, J. A., and Casdagli, M., 1991, "Embedology," *J. Stat. Phys.*, **65**(3-4), pp. 579–616.
- [25] Fraser, A. M., and Swinney, H. L., 1986, "Independent Coordinates for Strange Attractors from Mutual Information," *Phys. Rev. A*, **33**(2), pp. 1134–1140.
- [26] Kennel, M. B., Brown, R., and Abarbanel, H. D. I., 1992, "Determining Embedding Dimension for Phase-Space Reconstruction Using a Geometric Construction," *Phys. Rev. A*, **45**(6), pp. 3403–3411.
- [27] Ott, E., 1993, *Chaos in Dynamical Systems*, Cambridge, New York.
- [28] Moon, F. C., and Holms, P., 1979, "A Magnetoelastic Strange Attractors, J. Sound Vib.", **65**(2), pp. 275–296.
- [29] Feeny, B. F., Yuan, C. M., and Cusumano, J. P., 2000, "Parametric Identification of an Experimental Magneto-Elastic Oscillator," *J. Sound Vib.* (accepted).
- [30] Friedman, J. H., Bentley, J. L., and Finkel, R., 1977, "An Algorithm for Finding Best Matches in Logarithmic Expected Time," *ACM Trans. Math. Softw.*, **3**(2), pp. 209–226.
- [31] Golnaraghi, M., Lin, D., and Fromme, P., 1995, "Gear Damage Detection using Chaotic Dynamics Techniques: A Preliminary Study," *Proc. of the 1995 ASME Des. Tech. Conf., Symposium on Time-varying Systems and Structures*, Boston, MA, Sep 17–20, pp. 121–127.
- [32] Craig, C., Neilson, D., and Penman, J., 2000, "The Use of Correlation Dimension in Condition Monitoring of Systems with Clearance," *J. Sound Vib.*, **231**(1), pp. 1–17.
- [33] Jiang, J. D., Chen, J., and Qu, L. S., 1999, "The Application of Correlation Dimension in Gearbox Condition Monitoring," *J. Sound Vib.*, **223**(4), pp. 529–541.
- [34] Logan, D. B., and Mathew, J., 2000, "Using the Correlation Dimension for Vibration Fault Diagnosis of Rolling Element Bearing—I. Basic Concepts," *Mech. Syst. Signal Process.*, **10**(3), pp. 241–250.
- [35] Rosenstein, M. T., Collins, J. J., and DeLuca, C. J., 1993, "A Practical Method for Calculating Largest Lyapunov Exponents From Small Data Sets," *Physica D*, **65**(1-2), pp. 117–134.